Fe-chitosan complexes for oxidative degradation of emerging contaminants in water: Structure, activity, and reaction mechanism

Journal of Hazardous Materials 408 (2021) 124662

Contents lists available at ScienceDirect

Journal of Hazardous Materials

journal homepage: www.elsevier.com/locate/jhazmat

Research paper

Fe-chitosan complexes for oxidative degradation of emerging contaminants in water: Structure, activity, and reaction mechanism

Giulio Farinelli [a], Andrea Di Luca [b], Ville R.I. Kaila [b], Mark J. MacLachlan [c,*], Alberto Tiraferri [a,*]

[a] Department of Environment, Land and Infrastructure Engineering (DIATI), Politecnico di Torino, Corso Duca degli Abruzzi 24, 10129 Turin, Italy
[b] Department of Biochemistry and Biophysics, Stockholm University, Svante Arrhenius väg 16C, 10691 Stockholm, Sweden
[c] Department of Chemistry, University of British Columbia, 2036 Main Mall, Vancouver, British Columbia, V6T 1Z1, Canada

ARTICLE INFO

Editor: Dr. Danmeng Shuai

Keywords:
Chitosan
Contaminants of emerging concern
Water treatment
Ferryl
Catalysis

ABSTRACT

Versatile and ecofriendly methods to perform oxidations at near-neutral pH are of crucial importance for processes aimed at purifying water. Chitosan, a deacetylated form of chitin, is a promising starting material owing to its biocompatibility and ability to form stable films and complexes with metals. Here, we report a novel chitosan-based organometallic complex that was tested both as homogeneous and heterogeneous catalyst in the degradation of contaminants of emerging concern in water. The stoichiometry of the complex was experimentally verified with different metals, namely, Cu(II), Fe(III), Fe(II), Co(II), Pd(II), and Mn(II), and we identified the chitosan-Fe(III) complex as the most efficient catalyst. This complex effectively degraded phenol, triclosan, and 3-chlorophenol in the presence of hydrogen peroxide. A putative ferryl-mediated reaction mechanism is proposed based on experimental data, density functional theory calculations, and kinetic modeling. Finally, a film of the chitosan-Fe(III) complex was synthesized and proven a promising supported heterogeneous catalyst for water purification.

1. Introduction

Chitosan (CS) is the deacetylated form of chitin in which a number of acetamide groups have been replaced with amine (-NH_2) groups (Rinaudo, 2006). Chitin is the second most abundant polysaccharide in nature, with the major source being crustacean shells (Ravi Kumar, 2000; Bellich et al., 2016). Since a large amount of the crustacean exoskeleton is readily available as a by-product of the seafood processing industry, the raw material for chitosan production is inexpensive, rendering the large-scale production of CS economically feasible from this renewable resource. Some of the attractive features of this biopolymer are its biodegradability, biocompatibility, and low toxicity (Vårum et al., 1997; Rhoades and Roller, 2000; Raafat and Sahl, 2009). A distinctive feature of CS from a chemical standpoint is the high density of amine groups at the C-2 positions. This feature enables chitosan to form stable complexes with metals, a property that is exceptional among biopolymers (Qin, 1993; Guibal, 2004; Qu et al., 2011; Guibal et al., 2014; Gritsch et al., 2018).

The ability of CS to complex elements has been mostly exploited in environmental applications for heavy metal adsorption from water streams (Li et al., 2009, 2016; Liu et al., 2013; Weng et al., 2013; Yu et al., 2013; Zhang et al., 2016). When considering instead the degradation of organic micropollutants from water, advanced oxidation processes are established techniques, but they are not always environmentally friendly or effective at near-neutral pH (Babuponnusami and Muthukumar, 2012; Diya'uddeen et al., 2012; Lee et al., 2007; Shukla et al., 2010; Wang et al., 2020). CS-metal complexes are promising in creating inexpensive and sustainable organometallic catalysts, which may be applied without modifying the pH of the contaminated streams (generally circumneutral). To date, very few literature reports have discussed the ability of CS-metal complexes to work as organometallic catalysts for the oxidative degradation of organic molecules in water (dyes, perchlorate, *etc.*) (Vincent et al., 2004; Rashid et al., 2015; Gao et al., 2016; Xie et al., 2016). For example, a modified form of chitosan was used as a metal ligand to promote the selective oxidation of hydrocarbons (Chang et al., 2002). Other researchers applied a CS-Pd system as a homogeneous reductant for the hydro dehalogenation of chlorophenols (Vincent et al., 2003). However, all these studies employed expensive and sometimes toxic metal complexes, with the obvious risks of inhibiting implementation for environmental applications.

A CS-metal complex may be used as both homogeneous and

* Corresponding authors.
E-mail addresses: mmaclach@chem.ubc.ca (M.J. MacLachlan), alberto.tiraferri@polito.it (A. Tiraferri).

https://doi.org/10.1016/j.jhazmat.2020.124662
Received 14 September 2020; Received in revised form 28 October 2020; Accepted 22 November 2020
Available online 24 November 2020

heterogeneous catalyst. Homogeneous oxidation is easily employable within a water treatment plant but with several limitations (Diya'uddeen et al., 2012; Mirzaei et al., 2017). Approaches based on heterogeneous processes would circumvent difficulties related to catalyst recovery and would reduce the amount of reagents needed to implement the oxidation. Most studies on heterogeneous oxidative processes based on CS as a bio-chelating agent report the use of this material in the form of powders, flakes, or gel beads, which are not easily deployed (Lee and Lee, 2010; Rashid et al., 2015; Hou et al., 2016). The use of films remains limited, despite the well-known ability of CS to form stable films (Tiraferri et al., 2014). Seyed Dorraji et al. (2015) reported the efficiency of wet-spun chitosan hollow fibers loaded with Fe_3O_4 nanoparticles in the degradation of dyes in water. However, the use of an iron ion instead of insoluble iron-based nanoparticles would allow easier regeneration of the catalytic core during applications.

Iron is the most abundant metal on Earth and its use in the ionic form in CS-based catalysts would be groundbreaking (Frey and Reed, 2012). However, the nature of the interaction between CS and the iron, especially Fe(III), is still amply debated, thus preventing further development of these materials (Hernández et al., 2008). Gamblin et al. (1998) suggested the formation of a cluster between the CS polymer and the Fe (III) ions without an effective coordination. Nevertheless, other investigations reached the opposite conclusion (Sreenivasan, 1996; Sipos et al., 2003). Bhatia and Ravi (2003) suggested the formation of a CS-Fe (III) complex that is either penta- or hexa-coordinated. Hernández et al. (2008) supported the latter thesis adding that the complexation takes place in a large pH range (from pH 2 to basic pH) and that the most stable form of the complex exists in the pH range 4–6. Moreover, Nieto et al. concluded that the ferric ion is coordinated with two chitosan residues, three molecules of water, and one chloride ion. These authors indicated that the chitosan-Fe(III) complex is a distorted octahedral complex due to the presence of ligands of different nature and exhibits an isomeric shift typical of high spin Fe(III) complexes with σ-donor ligands (Nieto et al., 1992). Despite these reports about the chitosan complex with iron, current knowledge is insufficient with respect to the reaction mechanism when a CS-Fe complex is used for the oxidative degradation of organic contaminants in water.

In this study, we propose CS-metal complexes both as homogeneous and heterogeneous organometallic catalysts. Specifically, we examine the detailed nature of the CS-Fe(III) complex, defining both the stoichiometry and the molecular structure of the polymer-metal complex through a combination of experiments and quantum chemical density functional theory calculations. We also evaluate the effectiveness of chitosan-metal complexes for the oxidative degradation of contaminants of emerging concern in water. The reaction mechanism is discussed and a novel CS-Fe(III) film is proposed as a cheap and sustainable supported heterogeneous catalyst.

2. Experimental

2.1. Materials

Triclosan and 3-chlorophenol were purchased from Oakwood Chemicals (Estill, SC, USA). All the other reagents were purchased from Sigma-Aldrich. The chitosan (CS) used in this study had low molecular weight and a deacetylation grade $\geq$ 75%. The measured CS solubility in water was 433 mg/L; more details about this determination can be found in Supplementary Material (SM, Text S1).

2.2. Preparation of the chitosan solid films

The protocol for the preparation of CS films was adapted from previous reports (Zeng and Ruckenstein, 1996; Cui et al., 2018). Briefly, to prepare pure CS films, a polymer solution was obtained with 2% w/w of CS and 2% w/w of acetic acid in water. A volume of 10 mL was then poured on a petri dish and allowed to dry at room temperature until constant weight was achieved. The film was immersed overnight in a sodium hydroxide solution (1 M) and then washed thoroughly with water. Films were also prepared in the presence of iron(III) and iron(II). Specifically, three different aqueous solutions were used: (a) 2% w/w of CS, 2% w/w of acetic acid, and $FeCl_3$ (13.8 mM); (b) 2% w/w of CS, 2% of acetic acid, and $FeSO_4$ (9.2 mM); (c) 2% w/w of CS, 2% w/w of acetic acid, and $FeCl_2$ (9.2 mM). The concentration of iron was chosen based on the stoichiometric ratios defined in preliminary experiments (vide infra). A volume of 10 mL of each of the three solutions was poured into a separate petri dish and dried in the oven at 80 °C for 4 h. The films were left overnight in 0.1 M sodium hydroxide, then dried in the oven at 80 °C for 4 h, and finally washed with ethanol. The residual ethanol was evaporated at room temperature until constant weight was achieved. All the films had a diameter of 54 mm and a thickness between 5 and 20 μm. To assess the stability of the CS-Fe(III) film, this was immersed in 10 mL of water for 20 min under gentle stirring. Aliquots of the supernatant at initial and final times were sampled and UV–Vis spectra were compared with the spectrum obtained with a solution of iron(III) to detect any leaching of the metal into solution.

2.3. Oxidation experiments: homogeneous conditions

Six metals were tested as central ion to form complexes with CS. They were: Cu(II); Fe(III); Fe(II); Co(II); Pd(II); Mn(II). The stoichiometry ratios between the central ion and a saturated solution of CS in water (433 mg/L) were first measured with UV–Vis titrations. The stoichiometric complexes were applied as organometallic catalysts in the oxidation of contaminants of emerging concern in water, namely, phenol (PhOH), triclosan (TCS), and 3-chlorophenol (3-CP). The oxidant was hydrogen peroxide. Initially, an appropriate amount of stock metal solution was added to 10 mL of a saturated CS solution in water. The obtained mixture was stirred for 5 min before starting the reaction in order to ensure the formation of the complex. Please note that UV titration suggested that the formation of the complex in solution occurred nearly instantly. Subsequently, the contaminant and the oxidant were added in this order. Preliminary oxidation tests were performed with a relative mass concentration ratio between metal, contaminant, and oxidant equal to 1:1:1. The low amount of oxidant allowed a better visualization of the relative efficiency of the different complexes. Further contaminant degradation experiments were then performed with a higher amount of oxidant (metal:contaminant:oxidant = 1:1:3 mass concentration ratio). More precisely, 1/3 of the total concentration of the oxidant was added in three separate steps, at time zero and then two more times each 20 min. The metal concentration refers to that at the equivalence point with a saturated chitosan solution (vide infra). The final reaction time for all the oxidation experiments was 1 h. All the reaction occurred at room temperature, at near-neutral pH, under magnetic stirring; the pH value remained nearly constant during the reaction.

2.4. Oxidation experiments: heterogeneous conditions

The CS-Fe(III, II) films obtained as described above were placed in contact with a solution of the target contaminant, PhOH. The oxidation tests occurred with a relative concentration ratio between catalyst, contaminant, and hydrogen peroxide of 1:0.5:0.5. The oxidant was added in one aliquot. The concentration of the metal salts, corresponding to the catalyst concentration, was 13.8 mM for $FeCl_3$; 9.2 mM for $FeSO_4$; 9.2 mM for $FeCl_2$. The reactions were conducted for 20 min at room temperature, at near-neutral pH, under slow magnetic stirring; the pH value remained nearly constant during the reaction. To rule out the possibility of PhOH adsorption onto the CS- Fe(III, II) films, these films were placed in contact with a PhOH solution in the absence of hydrogen peroxide under magnetic stirring and the same environmental conditions adopted during oxidation tests. The adsorption tests occurred with a relative ratio between metal, contaminant, and oxidant of 1:1:0.5.

2.5. Analytical methods

UV–Vis spectrophotometric measurements were performed using a Cary 5000 Scan double-beam instrument (Varian). The concentrations of contaminants in solution were monitored by high-performance liquid chromatography coupled with a diode array detector (HPLC-DAD). The formation of by-products during the oxidation reactions was monitored with a liquid chromatography coupled with a quadrupole mass detector (LC-MS). Further information about the analytical methods can be found in the SM (Text S2).

2.6. Modeling of the chitosan dimer conformations

To explore conformations adopted by CS that could chelate Fe ions, we first pre-screened the possible conformations adopted by a CS dimer. To this end, the free energy surface along two torsional angles of the ether bond (ϕ,ψ, Fig. 4a) was calculated using 2D-umbrella sampling (US) (Kästner, 2011). The CS model was modeled using GAFF parameters and generated using tleap (Wang et al., 2004, 2006). Simulations were performed with NAMD 2.13 (Phillips et al., 2005), using a generalized Born (GB) implicit solvent model ($\varepsilon = 80$), an integration step of 1 fs with Langevin dynamics ($\tau = 5\ ps^{-1}$) at $T = 298$ K, and by employing a cutoff distance for non-bonded interactions of 9 Å. 50 windows for each variable was used, giving in total $50 \times 50 = 2500$ simulations. A harmonic restraining potential with a force constant of 0.025 kcal $mol^{-1}degree^{-2}$ was used for the 2D-US and the dihedral space was scanned between − 180 and 180°. The resulting free energy profiles were obtained using the weighted histogram analysis method (WHAM) (Cossio-Pérez et al., 2019) with 5 ns sampling for each replica. The obtained 2D-free energy profile resembled the profile by Tsereteli and Grafmüller (2017) obtained using coarse-grained models.

2.7. Modeling of the chitosan-Fe complex

To generate the α and β chitosan-Fe complexes, an Fe(III) ion was coordinated within the chitosan framework with the amino/hydroxyl/ether groups, and the amino/hydroxyl groups, respectively (see Fig. 4a). The ionic coordination spheres were saturated with water molecules (three for α− chitosan, four for β−chitosan), and the resulting structures were optimized at the DFT level using TPSSh/def2-SVP (Fe def2-TZVP) (Staroverov et al., 2003; Tao et al., 2003; Weigend and Ahlrichs, 2005). The aqueous surroundings was treated using the conductor-like screening model (COSMO) with an ε set to 80 (Schäfer et al., 2000). As an intermediate step, we optimized the structures in the high spin S= 5/2 Fe(III) state, followed by generation of the ferryl (Fe(IV)=O) species, by deprotonating a water molecule bound to the iron, and optimizing the structure at the same theory level in the $S = 1$ and $S = 2$ states, resulting in 14 structures (3 α and 4 β structures for the two respective spin states). Stable ground state structures were validated by computing the molecular Hessian, and single point energy calculations were performed at the TPSSh/def2-TZVPP/$\varepsilon = 80$ level. For modeling the ferryl species, the amino groups of the CS monomers were modeled in their neutral (-NH_2) states. All quantum chemical calculations were performed with TURBOMOLE v. 7.2 (Ahlrichs et al., 1989; Häser and Ahlrichs, 1989).

2.8. Kinetic model of reaction

To interpret the results obtained from oxidation experiments and understand whether a metal-based or a free-radical oxidation mechanism is dominant, a kinetic model was applied to simulate the oxidation of an organic species (Orange II) by H_2O_2 catalyzed by CS-Fe(II, III) complexes. The initial concentrations of H_2O_2, Orange II, and CS-Fe(II) or CS-Fe(III) complex were set at 10^{-4} M, mimicking the experimental setup. The kinetic model was created using COPASI 4.23 (Hoops et al., 2006), generating the system of reactions listed in Table S1 of the SM.

(a)

Central Ion	Equivalence Point
Cu(II)	~300 μM
Fe(III)	~300 μM
Fe(II)	~200 μM
Co(II)	~200 μM
Pd(II)	N.D.
Mn(II)	~150 μM

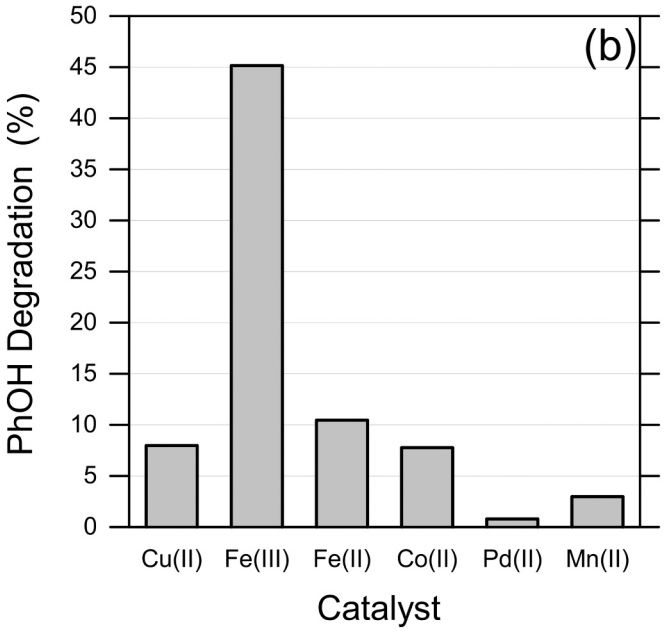

Fig. 1. Stoichiometry of the metal-chitosan complexes. (a) Metal concentration of saturation (equivalence point) in the CS-metal complexes at a chitosan concentration of 433 mg/L, from UV titration. (b) Phenol (PhOH) degradation resulting from the use of different CS-metal complexes as homogeneous catalysts after one addition of H_2O_2. The reaction was performed with metal:PhOH:H_2O_2 = 1:1:1 mass concentration ratio, and metal concentration as in (a).

The reaction constants (k_i) were chosen based on values reported in the literature (De Laat and Gallard, 1999; Kiwi et al., 2000; Chahbane et al., 2007). The system was simulated for 150 s with a time step of 15 ms, using a deterministic (LSODA) integration method. The reactions were simulated by varying each kinetics constant, k_i, individually over much wider range than realistically possible, from 10^{-4} to $10^{10}\ s^{-1}$ divided by 30 logarithmic intervals, and keeping all the other constants equal to the values reported in the literature (Table S1). To probe the difference in oxidation pathway promoted by Fe(II)- or Fe(III)-based catalysts, we started each model simulation with only one of the two ionic species (with two sets of simulations performed, one for each initial species), and observed the time evolution of the substrate (Orange II) and of two more products, one associated with the metal-based mechanism (referred to as “ferryl”) and the other with the free-radical mechanism (referred to as “free radical”).

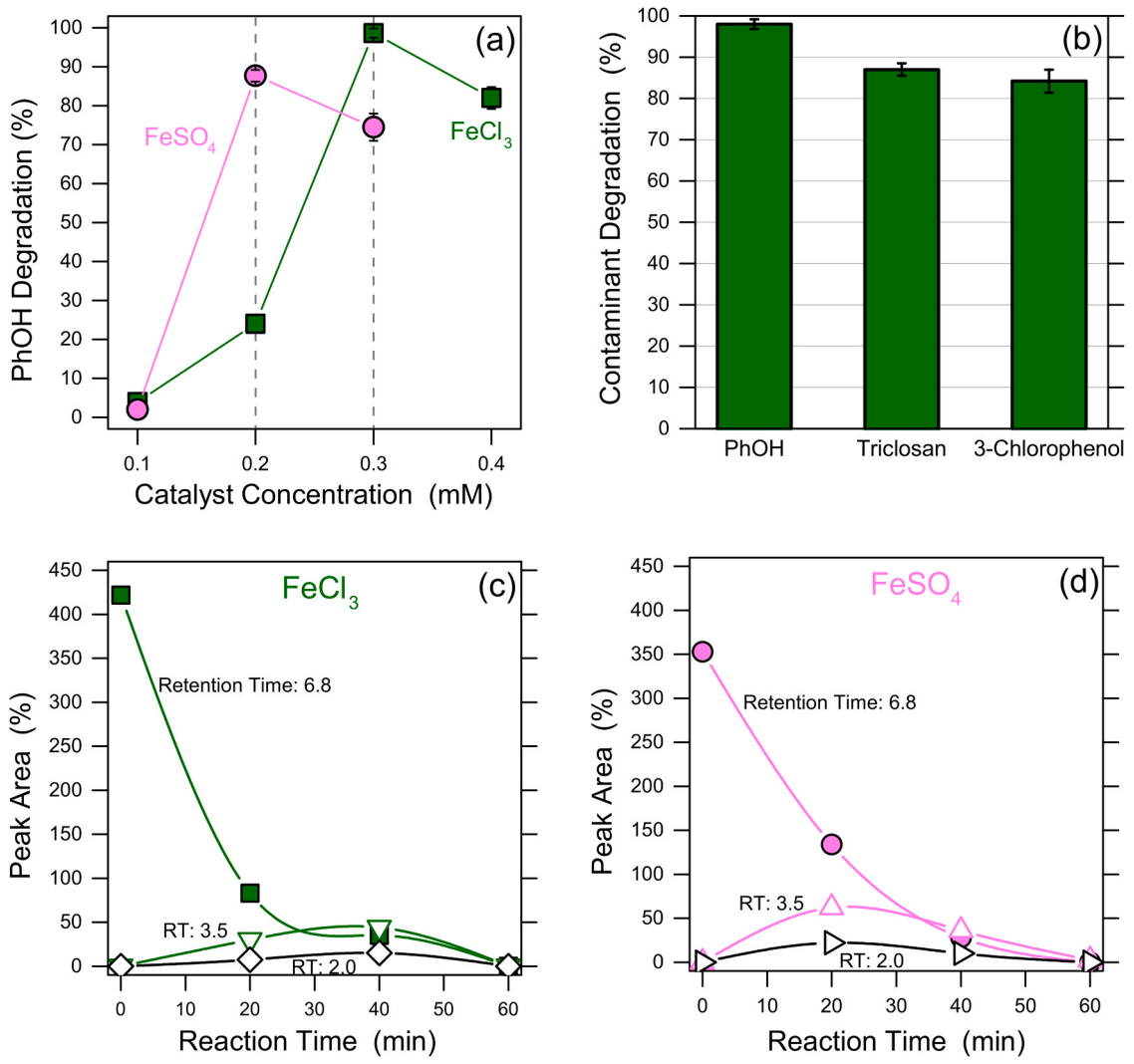

Fig. 2. Chitosan-Fe complexes in the degradation of organic contaminants. (a) Influence of metal concentration in the CS-Fe(III, II) complexes (CS concentration 433 mg/L) used as homogeneous catalysts for phenol (PhOH) degradation. (b) Degradation of three contaminants of emerging concern with the use of the CS-Fe(III) complex as homogeneous catalyst. (c, d) Degradation of PhOH and formation of byproducts monitored with LC-MS using (c) the CS-$FeCl_3$ complex or (d) the CS-$FeSO_4$ complex as homogeneous catalyst. The byproducts were identified as bi-hydroxylated compounds (e.g., catechol, resorcinol). The reactions were performed with metal:contaminant:H_2O_2 = 1:1:3 mass concentration ratio, and metal concentration as in Fig. 1a. The same conditions were applied to conduct the reactions using the CS-$FeCl_3$ complex related to (a-c). The reaction conditions with the CS-$FeSO_4$ complex were adjusted (metal:phenol:H_2O_2 = 1:1:30 mass concentration ratio) to obtain the same kinetics of degradation observed in the CS-$FeCl_3$ complex. The lines connecting the data points are intended only as a guide for the eye.

3. Results and discussion

3.1. Chitosan-metal interaction and catalytic efficiency of the complex

When catalysis occurs through an organometallic compound, the correct metal/ligand ratio allows maximization of the catalytic efficiency while avoiding free species in solution that may negatively impact the process (Farinelli et al., 2020). To determine the CS-metal binding stoichiometry, intended here as the ratio between the concentration of CS (g/L) and the concentration of the central ion (μM), UV–Vis titrations were performed with different metals as catalytic core, namely, Cu(II), Fe(III), Fe(II), Co(II), Pd(II), and Mn(II). Fig. 1a reports the concentration of the various metals associated to each equivalence point, that is, the inflection point of the titration curve, in a saturated aqueous solution of CS (433 mg/L); see Fig. S1 in the SM for the titration curves. The equivalence point was not reached for Pd, possibly because this metal forms clusters rather than complexes with chitosan.

The concentrations in Fig. 1a were thus applied to prepare the catalysts employed in preliminary homogeneous oxidation reactions aimed at the degradation of phenol (PhOH) in water. Fig. 1b shows the percentage of degraded substrate after one addition of a low amount of H_2O_2, to better assess the relative efficiency of the different catalysts. The highest efficiency was obtained with the two CS-Fe systems. The different efficiency observed with the Fe(III) and Fe(II) complexes may be possibly interpreted as due to a different reaction pathway, hence a different reaction mechanism, a hypothesis that was further investigated and that is discussed below.

3.2. Homogeneous degradation of contaminants by CS-Fe complexes

The activity of the most efficient CS-Fe(III) complex and that of the CS-Fe(II) complex were further examined with the goal to gain insight into their reaction efficiency and mechanisms. The results reported in Fig. 2a indicate that the maximum oxidation power of both complexes indeed corresponded with the stoichiometric metal concentration, namely, 200 μM and 300 μM for Fe(II) and Fe(III), respectively. The lower oxidation efficiency of the super-stoichiometric conditions may be rationalized with consumption of the oxidant (H_2O_2) by the excess

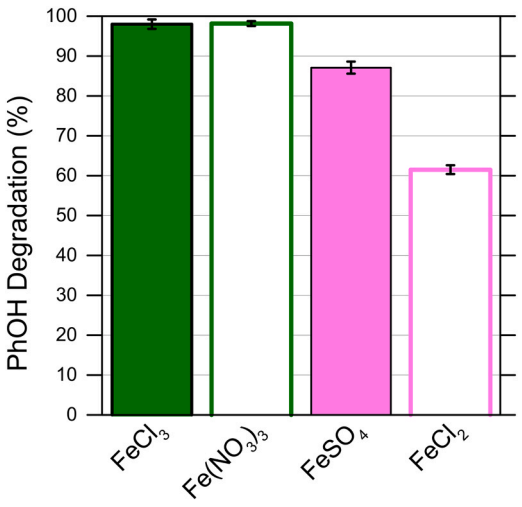

Fig. 3. Phenol degradation resulting from the use of CS-Fe(III, II) complexes applied as homogeneous catalysts obtained with different iron salts ($FeCl_3$, $Fe(NO_3)_3$, $FeSO_4$, $FeCl_2$). The reactions were performed with metal:PhOH:H_2O_2 = 1:1:3 mass concentration ratio, and metal concentration as in Fig. 1a.

species, while in the case of sub-stoichiometric metal with a low activity of the catalytic core.

When the CS-Fe(III) complex at optimal CS/metal ratio was applied for the homogeneous oxidation of three contaminants of emerging concern, PhOH, triclosan (TCS), and 3-chlorophenol (3-CP), the percentage of removal was always higher than 80%; see Fig. 2b. Please note that removal of PhOH by adsorption can also be ruled out based on the result presented in the SM (Fig. S4). The capability of the complex to degrade phenol more rapidly and efficiently than chlorinated compounds, namely, triclosan and 3-chlorophenol, is consistent with an oxidation reaction, which usually works through electrophilic transient species and is more effective in the degradation of electron-rich compounds (Miklos et al. 2018). Fig. S2 of the SM presents the time trends observed in the degradation of the three contaminants in the presence and in the absence of homogeneous catalysts and as a function of the catalyst concentration. These data suggest a sustained degradation rate within 60 min and the absence of contaminant removal when the only oxidant was present in solution. Please note that complete mineralization of the compounds was not reached in the experiments and was not the main goal of this study. The time evolution of the concentration of by-products was also analyzed during the degradation of PhOH; see Fig. 2c, d. Comparison of the maximum concentration elution time (t_{max}) of the by-products shows an important difference between the two systems, with the Fe(III)-based system being slower than the Fe(II) one, another indirect evidence suggesting that two different mechanisms of reaction may be at play.

3.3. *Insights into the reaction mechanism and the nature of the active species*

Fig. 3 summarizes the results obtained in the homogeneous-phase degradation of PhOH using different iron salts as catalytic core in the CS-Fe complex. The time trends observed in these experiments are presented in Fig. S3 of the SM and corroborate the occurrence of a sustained and near constant oxidation rate toward PhOH degradation within 60 min of reaction. In the case of Fe(II) as central ion, a significant increase in the efficiency of degradation of phenol with SO_4^{2-} as the counter-ion was observed with respect to Cl^-. On the other hand, no difference was detected when Fe(III) was the central ion, regardless of the counterion. Chloride ions directly scavenge $^{\bullet}OH$ with the formation of less reactive $Cl_2^{\bullet-}$ radicals (Kiwi et al., 2000). Therefore, it is possible to hypothesize that free radicals are the main reactive oxygen species in the oxidation mediated by Fe(II) as the central ion, whereas the prominent mechanism related to the CS-Fe(III) system is most likely the metal-based one.

An oxidation reaction can occur either through a free-radical or a metal-based mechanism, or a combination of the two (De Laat and Gallard, 1999; Kiwi et al., 2000; Pignatello et al., 2006). In the case of a free-radical mechanism similar to the Fenton reaction, chloride ions may scavenge the hydroxyl radical, while nitrate is an excellent counter-ion as (i) it does not complex ferric ions, therefore not suppressing their reaction with hydrogen peroxide, and (ii) it does not react with hydroxyl radicals (Lu and Chen, 1997; Pignatello et al., 2006). Sulfate is also a suitable counter-ion for free radical-based reactions: although this ion may slightly retard the redox reaction by coordinating to iron, the presence of other competitive ligands, such as CS itself, would thwart this effect (Pignatello, 1992; Pignatello et al., 2006). In contrast, during a metal-based reaction, the organometallic complexes generate an iron-oxo species (Fe^x =O), which may not be affected by the typical scavengers of a Fenton process (Ghosh et al., 2008; Beach et al., 2009; Farinelli et al., 2019).

If a metal-based reaction mechanism is dominant, this system requires the formation of a CS-ferryl species during the reaction cycle. To derive the possible structure of such putative CS-bound ferryl species, we performed both classical free energy exploration of the CS-framework and quantum chemical DFT calculations to explore the electronic structure of the CS-ferryl species. First, possible conformations accessible by the CS in the polymer chain were identified using a chitosan dimer. We identified three free energy minima (α, β, γ, Fig. 4a) that are similar to structures also previously described (Cunha et al., 2012; Tsereteli and Grafmüller, 2017). While both the α and β CS-complexes can chelate a metal ion by their amino and hydroxyl groups, the γ−structure was discarded due to its inability to form stable bidentate iron-complex. Structures similar to those presented here were also adopted in previous CS-metal studies (Braier and Jishi, 2000). The two candidate conformations were thus further employed to build a water-saturated complex of iron and optimized at the DFT level (see Section 2).

The DFT calculations involving the dimer-iron interaction suggest that the optimized complexes have typical structures and spin distributions observed for non-heme Fe(IV)=O species (Ghosh et al., 2004; Mader et al., 2018), corroborating the possibility of a metal-based reaction mechanism involving a ferryl species (see Fig. 4b). We did not identify a strong preference for a particular spin-state, with nearly degenerate S= 1 and S= 2 states, nor for a specific Fe(IV)=O orientation with respect to the CS polymer, suggesting an intrinsic diversity of the oxidation sites in the material (see Fig. S7). However, due to the high flexibility and heterogeneity of the starting CS polymer, a large number of CS-Fe complexes are possible, for example, a complex formed by the amino groups of two-non adjacent CS units (chains). Such structural heterogeneity may further modify the properties of the oxidant species by altering the ligand field of the complex, and thus the spin and stability (Kazaryan and Baerends, 2015) with respect to the structures explored in this study that comprise a single amino-group bound to the central iron. It is important to note that the DFT calculation was not used to define the exclusive occurrence one of the two mechanisms (free-radical; metal-based), but to verify the actual possibility of the presence of a ferryl species during the process, from a structural standpoint.

Further support of the two reaction mechanisms involving the CS-Fe (II, III) catalysts were separately obtained with a kinetic model applied to investigate the effect of the reaction constants (k_i) on the development of the system. Our set of reactions (see SM, Table S1) involved interchange of Fe(II) and Fe(III) species through a series of potential radical-based or ferryl-based reaction pathways (De Laat and Gallard, 1999; Kiwi et al., 2000; Chahbane et al., 2007). Fig. 4 reports the results obtained in the two systems starting from Fe(II) or Fe(III) as a function of k_1, (Fe(II) + H_2O_2 → Fe(III) + $^{\bullet}OH$ + OH^-). Here, the products generated via metal-based or free-radical reaction are referred to as ferryl and free

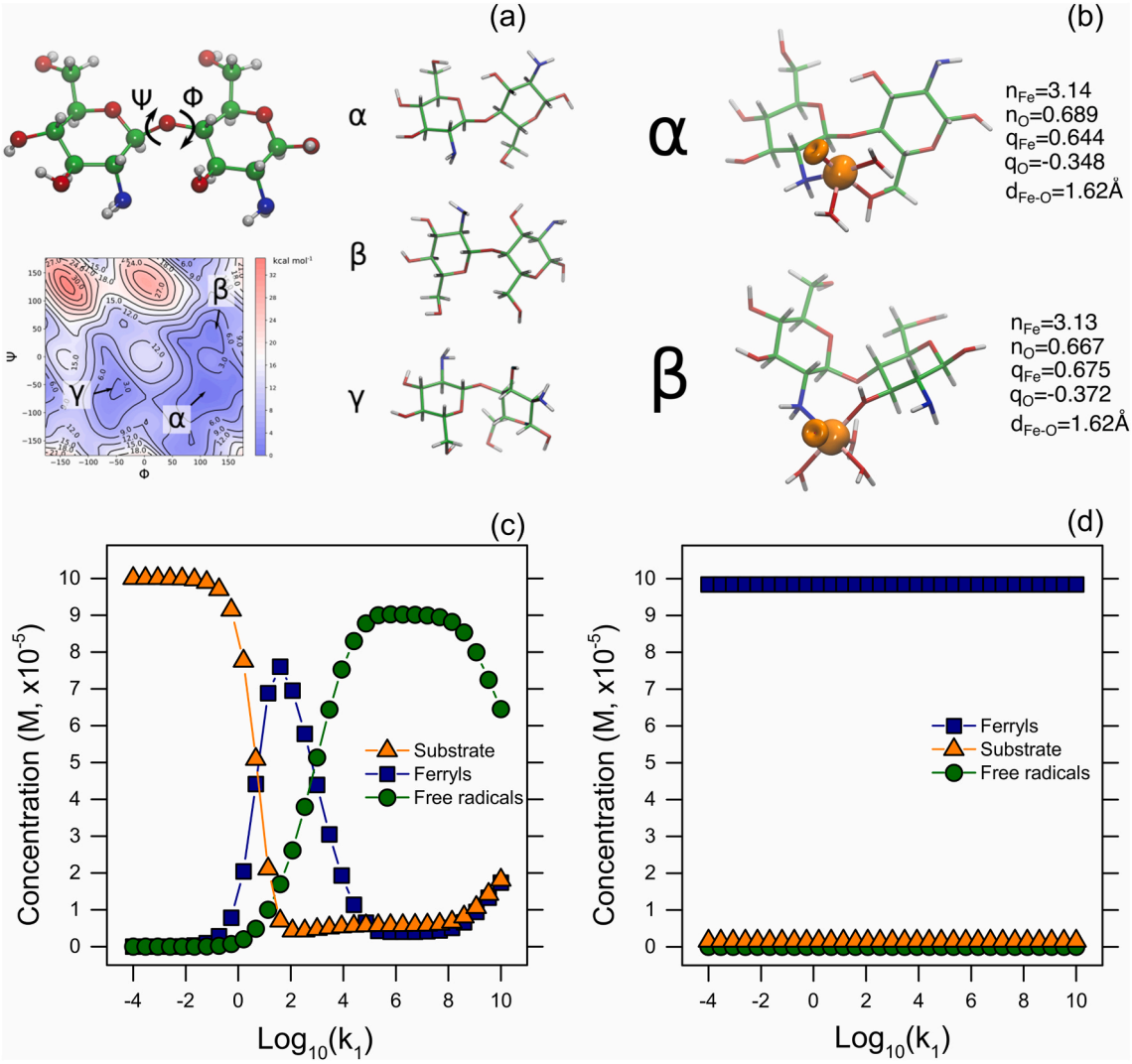

Fig. 4. Modeling of the chitosan-Fe complexes as catalysts. (a) Free-energy surface of the CS dimer along the ϕ and ψ torsional angles (see Methods). Three minimum free-energy structures (α, β, γ) identified are indicated on the right. The α and β CS-structures were further used to study the structure of the catalytic species. (b) Molecular structure of a ferryl species optimized at the DFT level (TPSSh/def2-TZVP) in the α and β conformations. The spin density distribution (at the TPSSh/def2-TZVP level) is shown as in surface representation at + 0.05 (−0.05) isovalue for α (β) spin density. Kinetic models for (c) Fe^{2+} and (d) Fe^{3+}. In c and d, the substrate, ferryl, and the free radical lines are related to the trend of Orange II, metal-based product, and free-radical product, respectively, obtained in the simulation. The lines connecting the data points are intended only as a guide for the eye.

radical, respectively, and indicated with blue squares and green circles in Fig. 4c,d. The model predicted the generation of both hydroxyl radicals and of Fe(III) ions starting from Fe(II) (see Fig. 4c and Reaction 1 in Table S1). Specifically, an increase of the reaction constant, k_1, produced a switch from a metal-based to a Fenton-like mechanism, with both ferryl and radical species co-existing under some conditions. In addition, by sufficiently slowing down the reaction ($k < 1\ s^{-1}$), the model outcome suggests that the process would be too slow to show any oxidation within the simulation time (150 s). In stark contrast, by starting the process with Fe(III) ions, the model predicted that the system would freely oxidize the substrate via a metal-based reaction and proceed to completion within the simulation time, regardless of the value of k_1 (Fig. 4d).

To account for uncertainties in the choice of reaction parameters adopted in the kinetic model, the prevailing species were monitored by scanning an ample range of nine different k_i values (Fig. S5 in the SM). Also, we performed additional calculations by fixing the value of k_1 at $10^4\ s^{-1}$ (instead of the most realistic value of 53 s^{-1}) (Kiwi et al., 2000), as well as testing the introduction of a direct reaction from Fe(II) to ferryl species (Reaction 17 in Table S1 of the SM). A similar pattern was found for all the reactions, with systematic differences in the species outcome using Fe(II) or Fe(III) as initial metals, thus implying a different progression of the reaction in terms of intermediates, hence mechanism of oxidation. Please note that the kinetic model was studied by taking into account general free radical and metal-based systems, and not specifically the system of this work. This model was thus deployed with the intent to evaluate the possible mechanism disagreement between systems starting with Fe^{2+} or with Fe^{3+}.

The results confirmed that divergence is possible among the two systems, with that starting from Fe(III) ions unlikely to give rise to a significant concentration of hydroxyl radicals. Overall, the indirect experimental observations that suggested a difference in the oxidation pathway in the CS-Fe(II) and CS-Fe(III) were supported by both DFT calculation and a kinetic model, which indicate respectively the possibility of formation of a ferryl species in the CS-Fe(III) complex and the unlikelihood of oxidation via hydroxyl radicals in the same system. These combined observations lead us to surmise that the CS-Fe(III) catalyst may promote a metal-based oxidation via ferryl species, $Fe^x = O$.

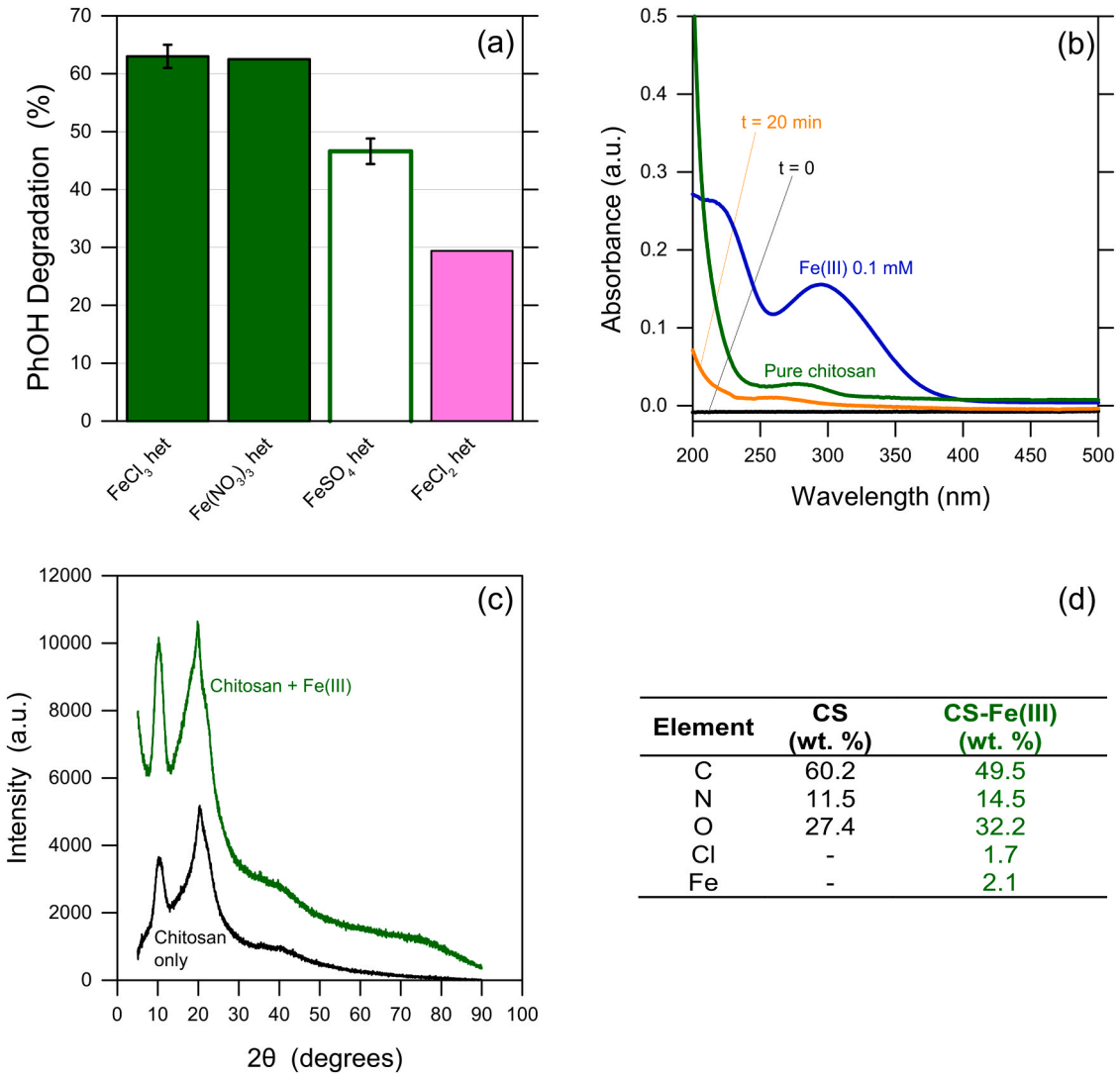

Element	CS (wt. %)	CS-Fe(III) (wt. %)
C	60.2	49.5
N	11.5	14.5
O	27.4	32.2
Cl	-	1.7
Fe	-	2.1

Fig. 5. CS-Fe complexes as heterogeneous catalysts. (a) Phenol degradation resulting from the use of CS-Fe(III, II) films applied as heterogeneous catalysts obtained with different iron salts, i.e., $FeCl_3$, $Fe(NO_3)_3$, $FeSO_4$, or $FeCl_2$. The films were obtained from an initial solution containing 2% chitosan in the presence of $FeCl_3$ = 13.8 mM, $Fe(NO_3)_3$ = 13.8 mM, $FeSO_4$ = 9.2 mM, or $FeCl_2$ = 9.2 mM. The reactions were performed with metal:PhOH:H_2O_2 = 1:0.5:0.5 mass concentration ratio, and metal concentration as in Fig. 1a. The oxidant was added in one aliquot. (b) Evaluation of leaching of Fe(III) from the surface of the CS-Fe(III) film. The blue and the green line represent the reference spectra of Fe(III) 0.1 mM and CS. (c) XRD and (d) EDX analyses of the surface of a pure chitosan film and of a CS-Fe(III) film. (For interpretation of the references to color in this figure legend, the reader is referred to the web version of this article.)

3.4. CS-Fe(III) as heterogeneous catalytic material

The final goal of this study is to propose a supported heterogeneous catalyst, which would offer several advantages compared to catalytic reaction performed under homogeneous conditions. For example, the latter would necessitate a catalyst recovery step downstream of the oxidation, without which chitosan may represent a TOC contamination in the effluent solution. Free radicals can easily degrade a polymeric material used as heterogeneous catalyst, hence degrade CS and negatively impact the process (Hsu et al., 2002; Erkselius and Karlsson, 2005). On the other hand, ferryl species are coordinated on the structure of the catalytic material itself. Therefore, a metal-based mechanism could be highly advantageous for heterogeneous catalysis. Based on the results discussed so far, the CS-Fe(III) system may thus be applied to form an effective solid-phase catalyst to support heterogeneous oxidation (see Fig. S6 of the SM for photographic images of representative films). Fig. 5a shows the degradation of phenol obtained using CS-Fe catalytic films, prepared from different iron salts. The contaminant removal activity of $FeCl_3$ or $FeSO_4$ films was not based on adsorption but on catalytic degradation, as shown in Fig. S4 of the SM. The results suggest that the efficiency of reaction and the effect of the counterions on the heterogeneous reaction are comparable with those observed in the homogeneous case. Therefore, the following two main inferences may be proposed: (i) the most likely reaction mechanisms are the same in the two phases, namely, metal-based in the CS-Fe(III) system and free radical-based in the with CS-Fe(II) system. This assumption is further supported by the faster degradation of the catalytic film observed with CS-Fe(II) supported catalyst. (ii) CS-Fe(III) films work as effective catalytic material for the degradation of organic contaminants in water. The catalytic films prepared with either $FeCl_3$ or $FeSO_4$ were also tested in a second cycle of reaction to evaluate the permanence of their degradation capability. The results presented in Fig. S8 of the SM corroborate the observations about the capability of the material to degrade contaminants. The relative loss of efficiency may be mainly attributed to the stability of the chitosan-based material.

To preliminarily assess the stability of the catalytic films, leaching experiments were performed, indicating that some CS was indeed released into solution; see Fig. 5b. This observation implies that the

polymeric matrix should be better stabilized, for example with the use of cross-linking agents. However, the absence or minor occurrence of iron leaching suggests that the CS-Fe(III) coordination was strong and any significant parasitic reactions during the degradation tests due to free iron in solution can be ruled out. Please note that it is not possible to completely exclude the occurrence of homogeneous reactions in solution due to leached CS-Fe(III) complex, but leaching was sufficiently low to assume a minor role of the homogeneous process in the degradation of PhOH in the presence of the supported catalyst. Fe(III) may also be oxidized to Fe_nO_x during the preparation of the material or during the oxidation reaction. The potential presence of iron oxide nanoparticles may thus also affect the results. Fig. 5c shows the XRD characterization of a simple CS film (black line) and the CS-Fe(III) film (green line) after the oxidation reaction. Both lines display only the two characteristic peaks of CS (Nagahama et al., 2009; Cui et al., 2018). This implies that no other solid compounds are present in the material and that the oxidation was thus promoted uniquely by the CS-Fe(III) coordination. From SEM analysis (see Fig. S6 in the SM), both the CS and the CS-Fe(III) materials appeared as dense films composed by the overlap of thin layers. Fig. 5d summarizes the elemental composition, which confirmed the presence of the iron ion in the CS-Fe(III) film.

4. Conclusions

Chitosan-metal coordination systems with different metallic cores were tested as potential organometallic catalysts for the degradation of phenol in water. Fe(III) was found to form an effective catalytic complex, a promising candidate for practical applications by virtue of the low cost and environmental impact of Fe(III). The CS-Fe(III) catalyst was also able to degrade (> 80% removal) triclosan and 3-chlorophenol in the homogeneous phase in 1 h and in the presence of hydrogen peroxide. An in-depth investigation combining experiments, simulations of the complex structure, and a kinetic reaction model, suggested that the CS-Fe(III) system is a robust polymer-metal complex that promotes oxidation through a metal-based (ferryl mediated) mechanism. On the other hand, the CS-Fe(II) system likely works through a mixed free radical and metal-based reaction mechanism.

The CS-Fe(III) system was also tested as a solid catalytic film for heterogeneous reaction. The results suggest that the solid catalyst also works through a metal-based mechanism, which is necessary to perform a stable heterogeneous catalytic process, and that its catalytic effectiveness has significant potential for the removal of organic contaminants in water. In conclusion, this work proved the ability of a biodegradable, environmentally friendly, cheap and easy-to-use system (CS-Fe(III) system) to work as a catalyst toward the degradation of contaminants of emerging concern in water. This catalyst is active at near-neutral pH and promotes oxidation via ferryl species: these conditions are particularly advantageous as they allow the elimination of pH-adjusting chemicals before and after oxidation and as they provide better control over the degradation products compared to traditional free radical-based oxidation. To develop the supported heterogeneous catalyst, optimization of the material should be specifically directed toward the synthesis of a more stable catalytic film in water, for example with the use of cross-linking agents.

CRediT authorship contribution statement

Giulio Farinelli: Conceptualization, Data curation, Formal analysis, Investigation, Methodology, Visualization, Writing - original draft. **Andrea Di Luca**: Data Curation, Formal analysis, Investigation, Visualization, Writing - original draft. **Ville R.I. Kaila**: Resources, Supervision, Validation, Writing - review & editing. **Mark J. MacLachlan**: Resources, Supervision, Writing - review & editing. **Alberto Tiraferri**: Funding acquisition, Project administration, Supervision, Visualization, Writing - review & editing.

Declaration of Competing Interest

The authors declare that they have no known competing financial interests or personal relationships that could have appeared to influence the work reported in this paper.

Acknowledgments

G.F. thanks Politecnico di Torino for financial support during his mobility at the University of British Columbia. A.T. thanks Politecnico di Torino for financial support (grant 58_RRI19TIRALB). The authors thank Francesco D'Acierno for providing training and technical assistance to G.F. and for providing the SEM image of Fe-chitosan film in the SI.

Appendix A. Supporting information

Supplementary data associated with this article can be found in the online version at doi:10.1016/j.jhazmat.2020.124662.

References

Ahlrichs, R., Bär, M., Häser, M., Horn, H., Kölmel, C., 1989. Electronic structure calculations on workstation computers: the program system turbomole. Chem. Phys. Lett. 162, 165–169. https://doi.org/10.1016/0009-2614(89)85118-8.

Babuponnusami, A., Muthukumar, K., 2012. Advanced oxidation of phenol: a comparison between Fenton, electro-Fenton, sono-electro-Fenton and photo-electro-Fenton processes. Chem. Eng. J. 183, 1–9. https://doi.org/10.1016/j.cej.2011.12.010.

Beach, E.S., Duran, J.L., Horwitz, C.P., Collins, T.J., 2009. Activation of hydrogen peroxide by an Fe-TAML complex in strongly alkaline aqueous solution: homogeneous oxidation catalysis with industrial significance. Ind. Eng. Chem. Res. 48, 7072–7076. https://doi.org/10.1021/ie9005723.

Bellich, B., Agostino, I.D., Semeraro, S., Gamini, A., Cesàro, A., 2016. The good, the bad and the ugly" of chitosans. Mar. Drugs 14, 99. https://doi.org/10.3390/md14050099.

Bhatia, S.C., Ravi, N., 2003. A Mössbauer study of the interaction of chitosan and D-glucosamine with iron and its relevance to other metalloenzymes. Biomacromolecules 4, 723–727. https://doi.org/10.1021/bm020131n.

Braier, N.C., Jishi, R.A., 2000. Density functional studies of Cu^{2+} and Ni^{2+} binding to chitosan. J. Mol. Struct. Theochem. 499, 51–55. https://doi.org/10.1016/S0166-1280(99)00288-2.

Chahbane, N., Popescu, D.-L., Mitchell, D.A., Chanda, A., Lenoir, D., Ryabov, A.D., Schramm, K.-W., Collins, T.J., 2007. FeIII–TAML-catalyzed green oxidative degradation of the azo dye orange II by H_2O_2 and organic peroxides: products, toxicity, kinetics, and mechanisms. Green Chem. 9, 49–57. https://doi.org/10.1039/B604990G.

Chang, Y., Wang, Y., Su, Z., 2002. Preparation of chitosan-bound nitrobenzaldehyde metal complexes and studies on its catalytic oxidative activity and reactive mechanism. J. Appl. Polym. Sci. 83, 2188–2194. https://doi.org/10.1002/app.10183.

Cossio-Pérez, R., Pierdominici-Sottile, G., Sobrado, P., Palma, J., 2019. Molecular dynamics simulations of substrate release from trypanosoma Cruzi UDP-galactopyranose mutase. J. Chem. Inf. Model. 59, 809–817. https://doi.org/10.1021/acs.jcim.8b00675.

Cui, L., Gao, S., Song, X., Huang, L., Dong, H., 2018. Preparation and Characterization of Chitosan. 28433–28439. https://doi.org/10.1039/c8ra05526b.

Cunha, R.A., Soares, T.A., Rusu, V.H., Pontes, F.J. S., Franca, E.F., Lins, R.D. (2012). The Molecular Structure and Conformational Dynamics of Chitosan Polymers: An Integrated Perspective from Experiments and Computational Simulations. The Complex World of Polysaccharides. D. N. Karunaratne, IntechOpen.

Diya'uddeen, B.H., Abdul Aziz, A.R., Daud, W.M.A.W., 2012. On the limitation of fenton oxidation operational parameters: a review. Int. J. Chem. React. Eng. 10 https://doi.org/10.1515/1542-6580.2913.

Erkselius, S., Karlsson, O.J., 2005. Free radical degradation of hydroxyethyl cellulose. Carbohydr. Polym. 62, 344–356. https://doi.org/10.1016/j.carbpol.2005.08.013.

Farinelli, G., Minella, M., Pazzi, M., Giannakis, S., Pulgarin, C., Vione, D., Tiraferri, A., 2020. natural iron ligands promote a metal-based oxidation mechanism for the Fenton reaction in water environments. J. Hazard. Mater. 393, 122413 https://doi.org/10.1016/j.jhazmat.2020.122413.

Farinelli, G., Minella, M., Sordello, F., Vione, D., Tiraferri, A., 2019. Metabisulfite as an unconventional reagent for green oxidation of emerging contaminants using an iron-based catalyst. ACS Omega 4, 20732–20741. https://doi.org/10.1021/acsomega.9b03088.

Frey, P.A., Reed, G.H., 2012. The ubiquity of iron. ACS Chem. Biol. 7, 1477–1481. https://doi.org/10.1021/cb300323q.

Gamblin, B.E., Stevens, J.G., Wilson, K.L., 1998. Structural investigations of chitin and chitosan complexed with iron or tin. Hyperfine Interact. 112, 117–122. https://doi.org/10.1023/A:1011001013953.

Gao, M., Zhang, D., Li, W., Chang, J., Lin, Q., Xu, D., Ma, H., 2016. Degradation of methylene blue in a heterogeneous Fenton reaction catalyzed by chitosan

crosslinked ferrous complex. J. Taiwan Inst. Chem. Eng. 67, 355–361. https://doi.org/10.1016/j.jtice.2016.08.010.
Ghosh, A., Mitchell, D.A., Chanda, A., Ryabov, A.D., Popescu, D.L., Upham, E.C., Collins, G.J., Collins, T.J., 2008. Catalase−peroxidase activity of iron(III)−TAML activators of hydrogen peroxide. J. Am. Chem. Soc. 130, 15116–15126. https://doi.org/10.1021/ja8043689.
Ghosh, A., Tangen, E., Ryeng, H., Taylor, Peter, R., 2004. Electronic structure of high-spin iron(IV) complexes. Eur. J. Inorg. Chem. 2004, 4555–4560. https://doi.org/10.1002/ejic.200400362.
Gritsch, L., Lovell, C., Goldmann, W.H., Boccaccini, A.R., 2018. Fabrication and characterization of copper(II)-chitosan complexes as antibiotic-free antibacterial biomaterial. Carbohydr. Polym. 179, 370–378. https://doi.org/10.1016/j.carbpol.2017.09.095.
Guibal, E., 2004. Interactions of metal ions with chitosan-based sorbents: a review. Sep. Purif. Technol. 38, 43–74. https://doi.org/10.1016/j.seppur.2003.10.004.
Guibal, E., Vincent, T., Navarro, R., 2014. Metal ion biosorption on chitosan for the synthesis of advanced materials. J. Mater. Sci. 49, 5505–5518. https://doi.org/10.1007/s10853-014-8301-5.
Häser, M., Ahlrichs, R., 1989. Improvements on the direct SCF method. J. Comput. Chem. 10, 104–111. https://doi.org/10.1002/jcc.540100111.
Hernández, R.B., Franco, A.P., Yola, O.R., López-Delgado, A., Felcman, J., Recio, M.A.L., Mercê, A.L.R., 2008. Coordination study of chitosan and Fe^{3+}. J. Mol. Struct. 877, 89–99. https://doi.org/10.1016/j.molstruc.2007.07.024.
Hoops, S., Gauges, R., Lee, C., Pahle, J., Simus, N., Singhal, M., Xu, L., Mendes, P., Kummer, U., 2006. COPASI - A COmplex PAthway SImulator. Bioinformatics 22, 3067–3074. https://doi.org/10.1093/bioinformatics/btl485.
Hou, P., Shi, C., Wu, L., Hou, X., 2016. Chitosan/Hydroxyapatite/Fe_3O_4 magnetic composite for metal-complex dye AY220 removal: recyclable metal-promoted Fenton-like degradation. Microchem. J. 128, 218–225. https://doi.org/10.1016/j.microc.2016.04.022.
Hsu, S.-C., Don, T.-M., Chiu, W.-Y., 2002. Free radical degradation of chitosan with potassium persulfate. Polym. Degrad. Stab. 75, 73–83. https://doi.org/10.1016/S0141-3910(01)00205-1.
Kästner, J., 2011. Umbrella sampling. Wiley Interdiscip. Rev. Comput. Mol. Sci. 1, 932–942. https://doi.org/10.1002/wcms.66.
Kazaryan, A., Baerends, E.J., 2015. Ligand field effects and the high spin–high reactivity correlation in the H abstraction by non-heme iron(IV)–oxo complexes: a DFT frontier orbital perspective. ACS Catal. 5, 1475–1488. https://doi.org/10.1021/cs501721y.
Kiwi, J., Lopez, A., Nadtochenko, V., 2000. Mechanism and kinetics of the OH-radical intervention during fenton oxidation in the presence of a significant amount of radical scavenger (Cl^-). Environ. Sci. Technol. 34, 2162–2168. https://doi.org/10.1021/es991406i.
De Laat, J., Gallard, H., 1999. Catalytic decomposition of hydrogen peroxide by Fe(III) in homogeneous aqueous solution: mechanism and kinetic modeling. Environ. Sci. Technol. 33, 2726–2732. https://doi.org/10.1021/es981171v.
Lee, Y., Lee, W., 2010. Degradation of trichloroethylene by Fe(II) chelated with cross-linked chitosan in a modified Fenton reaction. J. Hazard. Mater. 178, 187–193. https://doi.org/10.1016/j.jhazmat.2010.01.062.
Lee, C., Yoon, J., Von Gunten, U., 2007. Oxidative degradation of N-nitrosodimethylamine by conventional ozonation and the advanced oxidation process ozone/hydrogen peroxide. Water Res. 41, 581–590. https://doi.org/10.1016/j.watres.2006.10.033.
Liu, T., Yang, X., Wang, Z.-L., Yan, X., 2013. Enhanced chitosan beads-supported Fe0-nanoparticles for removal of heavy metals from electroplating wastewater in permeable reactive barriers. Water Res. 47, 6691–6700. https://doi.org/10.1016/j.watres.2013.09.006.
Li, A., Lin, R., Lin, C., He, B., Zheng, T., Lu, L., Cao, Y., 2016. An environment-friendly and multi-functional absorbent from chitosan for organic pollutants and heavy metal ion. Carbohydr. Polym. 148, 272–280. https://doi.org/10.1016/j.carbpol.2016.04.070.
Li, J.-M., Meng, X.-G., Hu, C.-W., Du, J., 2009. Adsorption of phenol, p-chlorophenol and p-nitrophenol onto functional chitosan. Bioresour. Technol. 100, 1168–1173. https://doi.org/10.1016/j.biortech.2008.09.015.
Lu, M.-C., Chen, J.-N., 1997. Effect of inorganic ions on the ozidation of dichlorvos insecticide with Fenton's reagent. Chemosphere 35, 2285–2293. https://doi.org/10.1016/S0045-6535(97)00307-X.
Mader, S.L., Bräuer, A., Groll, M., Kaila, V.R.I., 2018. Catalytic mechanism and molecular engineering of quinolone biosynthesis in dioxygenase AsqJ. Nat. Commun. 9, 1168. https://doi.org/10.1038/s41467-018-03442-2.
Miklos, D.B., Remy, C., Jekel, M., Linden, K.G., Drewes, J.E., Hübner, U., 2018. Evaluation of advanced oxidation processes for water and wastewater treatment – a critical review. Water Res. 139, 118–131. https://doi.org/10.1016/j.watres.2018.03.042.
Mirzaei, A., Chen, Z., Haghighat, F., Yerushalmi, L., 2017. Removal of pharmaceuticals from water by homo/heterogonous Fenton-type processes – a review. Chemosphere 174, 665–688. https://doi.org/10.1016/j.chemosphere.2017.02.019.
Nagahama, H., Maeda, H., Kashiki, T., Jayakumar, R., Furuike, T., Tamura, H., 2009. Preparation and characterization of novel chitosan/gelatin membranes using chitosan hydrogel. Carbohydr. Polym. 76, 255–260. https://doi.org/10.1016/j.carbpol.2008.10.015.
Nieto, J.M., Peniche-Covas, C., Del Bosque, J., 1992. Preparation and characterization of a chitosan-Fe(III) complex. Carbohydr. Polym. 18, 221–224. https://doi.org/10.1016/0144-8617(92)90067-Z.
Phillips, J.C., Braun, R., Wang, W., Gumbart, J., Tajkhorshid, E., Villa, E., Chipot, C., Skeel, R.D., Kalé, L., Schulten, K., 2005. Scalable molecular dynamics with NAMD. J. Comput. Chem. 26, 1781–1802. https://doi.org/10.1002/jcc.20289.
Pignatello, J.J., 1992. Dark and photoassisted Fe^{3+}-catalyzed degradation of chlorophenoxy herbicides by hydrogen peroxide. Environ. Sci. Technol. 26, 944–951. https://doi.org/10.1021/es00029a012.
Pignatello, J.J., Oliveros, E., MacKay, A., 2006. Advanced oxidation processes for organic contaminant destruction based on the fenton reaction and related chemistry. Crit. Rev. Environ. Sci. Technol. 36, 1–84. https://doi.org/10.1080/10643380500326564.
Qin, Y., 1993. The chelating properties of chitosan fibers. J. Appl. Polym. Sci. 49, 727–731. https://doi.org/10.1002/app.1993.070490418.
Qu, J., Hu, Q., Shen, K., Zhang, K., Li, Y., Li, H., Zhang, Q., Wang, J., Quan, W., 2011. The preparation and characterization of chitosan rods modified with Fe^{3+} by a chelation mechanism. Carbohydr. Res. 346, 822–827. https://doi.org/10.1016/j.carres.2011.02.006.
Raafat, D., Sahl, H.-G., 2009. Chitosan and its antimicrobial potential – a critical literature survey. Mol. Biotechnol. 2, 186–201. https://doi.org/10.1111/j.1751-7915.2008.00080.x.
Rashid, S., Shen, C., Chen, X., Li, S., Chen, Y., Wen, Y., Liu, J., 2015. Enhanced catalytic ability of chitosan–Cu–Fe bimetal complex for the removal of dyes in aqueous solution. RSC Adv. 5, 90731–90741. https://doi.org/10.1039/C5RA14711E.
Ravi Kumar, M.N.V., 2000. A review of chitin and chitosan applications. React. Funct. Polym. 46, 1–27. https://doi.org/10.1016/S1381-5148(00)00038-9.
Rhoades, J., Roller, S., 2000. Antimicrobial actions of degraded and native chitosan against spoilage organisms in laboratory media and foods. Appl. Environ. Microbiol. 66, 80–86. https://doi.org/10.1128/AEM.66.1.80-86.2000.
Rinaudo, M., 2006. Chitin and chitosan: properties and applications. Prog. Polym. Sci. 31, 603–632. https://doi.org/10.1016/j.progpolymsci.2006.06.001.
Schäfer, A., Klamt, A., Sattel, D., Lohrenz, J.C.W., Eckert, F., 2000. COSMO implementation in TURBOMOLE: extension of an efficient quantum chemical code towards liquid systems. Phys. Chem. Chem. Phys. 2, 2187–2193. https://doi.org/10.1039/b000184h.
Seyed Dorraji, M.S., Mirmohseni, A., Carraro, M., Gross, S., Simone, S., Tasselli, F., Figoli, A., 2015. Fenton-like catalytic activity of wet-spun chitosan hollow fibers loaded with Fe_3O_4 nanoparticles: batch and continuous flow investigations. J. Mol. Catal. A Chem. 398, 353–357. https://doi.org/10.1016/j.molcata.2015.01.003.
Shukla, P.R., Wang, S., Sun, H., Ang, H.M., Tadé, M., 2010. Activated carbon supported cobalt catalysts for advanced oxidation of organic contaminants in aqueous solution. Appl. Catal. B Environ. 100, 529–534. https://doi.org/10.1016/j.apcatb.2010.09.006.
Sipos, P., Berkesi, O., Tombácz St., E., Pierre, T.G., Webb, J., 2003. Formation of spherical Iron(III) oxyhydroxide nanoparticles sterically stabilized by chitosan in aqueous solutions. J. Inorg. Biochem. 95, 55–63. https://doi.org/10.1016/S0162-0134(03)00068-0.
Sreenivasan, K., 1996. Thermal stability studies of some chitosanmetal ion complexes using differential scanning calorimetry. Polym. Degrad. Stab. 52, 85–87. https://doi.org/10.1016/0141-3910(95)00220-0.
Staroverov, V.N., Scuseria, G.E., Tao, J., Perdew, J.P., 2003. Comparative assessment of a new nonempirical density functional: molecules and hydrogen-bonded complexes. J. Chem. Phys. 119, 12129–12137. https://doi.org/10.1063/1.1626543.
Tao, J., Perdew, J.P., Staroverov, V.N., Scuseria, G.E., 2003. Climbing the density functional ladder: nonempirical meta–generalized gradient approximation designed for molecules and solids. Phys. Rev. Lett. 91, 3–6. https://doi.org/10.1103/PhysRevLett.91.146401.
Tiraferri, A., Maroni, P., Caro Rodrìguez, D., Borkovec, M., 2014. Mechanism of chitosan adsorption on silica from aqueous solutions. Langmuir 30, 4980–4988. https://doi.org/10.1021/la500680g.
Tsereteli, L., Grafmüller, A., 2017. An accurate coarse-grained model for chitosan polysaccharides in aqueous solution. PLoS One 12, e0180938. https://doi.org/10.1371/journal.pone.0180938.
Vårum, K.M., Myhr, M.M., Hjerde, R.J.N., Smidsrød, O., 1997. In vitro degradation rates of partially n-acetylated chitosans in human serum. Carbohydr. Res. 299, 99–101. https://doi.org/10.1016/S0008-6215(96)00332-1.
Vincent, T., Peirano, F., Guibal, E., 2004. Chitosan supported palladium catalyst. VI. Nitroaniline degradation. J. Appl. Polym. Sci. 94, 1634–1642. https://doi.org/10.1002/app.21051.
Vincent, T., Spinelli, S., Guibal, E., 2003. Chitosan-supported palladium catalyst. II. Chlorophenol dehalogenation. Ind. Eng. Chem. Res. 42, 5968–5976. https://doi.org/10.1021/ie0301482.
Wang, J., Wang, W., Kollman, P.A., Case, D.A., 2006. Automatic atom type and bond type perception in molecular mechanical calculations. J. Mol. Graph. Modell. 25, 247–260. https://doi.org/10.1016/j.jmgm.2005.12.005.
Wang, J., Wolf, R.M., Caldwell, J.W., Kollman, P.A., Case, D.A., 2004. Development and testing of a general amber force field. J. Comput. Chem. 25, 1157–1174. https://doi.org/10.1002/jcc.20035.
Wang, J., Yoshida, A., Wang, P., Yu, T., Wang, Z., Hao, X., Abudula, A., Guan, G., 2020. Catalytic oxidation of volatile organic compound over cerium modified cobalt-based mixed oxide catalysts synthesized by electrodeposition method. Appl. Catal. B Environ. 271, 118941 https://doi.org/10.1016/j.apcatb.2020.118941.
Weigend, F., Ahlrichs, R., 2005. Balanced basis sets of split valence, triple zeta valence and quadruple zeta valence quality for H to Rn: design and assessment of accuracy. Phys. Chem. Chem. Phys. 7, 3297–3305. https://doi.org/10.1039/b508541a.
Weng, X., Lin, S., Zhong, Y., Chen, Z., 2013. Chitosan stabilized bimetallic fe/ni nanoparticles used to remove mixed contaminants-amoxicillin and Cd (II) from aqueous solutions. Chem. Eng. J. 229, 27–34. https://doi.org/10.1016/j.cej.2013.05.096.
Xie, Y., Yi, Y., Qin, Y., Wang, L., Liu, G., Wu, Y., Diao, Z., Zhou, T., Xu, M., 2016. Perchlorate degradation in aqueous solution using chitosan-stabilized zero-valent

iron nanoparticles. Sep. Purif. Technol. 171, 164–173. https://doi.org/10.1016/j.seppur.2016.07.023.
Yu, Z., Zhang, X., Huang, Y., 2013. Magnetic chitosan–iron(III) hydrogel as a fast and reusable adsorbent for chromium(VI) removal. Ind. Eng. Chem. Res. 52, 11956–11966. https://doi.org/10.1021/ie400781n.
Zeng, X., Ruckenstein, E., 1996. Control of pore sizes in macroporous chitosan and chitin membranes. Ind. Eng. Chem. Res. 35, 4169–4175. https://doi.org/10.1021/ie960270j.
Zhang, L., Zeng, Y., Cheng, Z., 2016. Removal of heavy metal ions using chitosan and modified chitosan: a review. J. Mol. Liq. 214, 175–191. https://doi.org/10.1016/j.molliq.2015.12.013.